LHCb-CONF-2010-013
December 10, 2010

Prompt charm production in pp collisions at $\sqrt{s} = 7\,\text{TeV}$

The LHCb Collaboration[1]

Abstract

Open charm production in inelastic pp collisions at a centre-of-mass energy $\sqrt{s} = 7\,\text{TeV}$ has been studied with the LHCb detector at the LHC using an integrated luminosity of $1.81\,\text{nb}^{-1}$. Cross-sections have been determined for $D^0/\overline{D}^0$, $D^{*\pm}$, $D^{\pm}$, and $D_s^{\pm}$ in bins of transverse momentum and rapidity in the region $0 < p_{\text{T}} < 8\,\text{GeV}/c$ and $2 < y < 4.5$. The results are compared with theoretical predictions and with expectations from the LHCb tuning of the PYTHIA generator. Good agreement both in shape and absolute normalisation is found. A direct comparison of $D_s^{\pm}$ and $D^{\pm}$ gives the cross-section ratio integrated over $2.0 < y < 4.5$ as $\sigma(D^+)/\sigma(D_s^+) = 2.32 \pm 0.27(\text{stat}) \pm 0.26(\text{syst})$. We find a total $c\bar{c}$ cross-section to produce c-flavoured hadrons in the range $0 < p_{\text{T}} < 8\,\text{GeV}/c$ and $2 < y < 4.5$ of $1.23 \pm 0.19\,\text{mb}$. Using PYTHIA to extrapolate the measurement to full phase space, a total cross-section $\sigma(pp \to c\bar{c}X) = 6.10 \pm 0.93\,\text{mb}$ is obtained.

[1]Conference note prepared for the 2010 Summer Conferences; contact authors: Michael Schmelling (Michael.Schmelling@mpi-hd.mpg.de) and Patrick Spradlin (Patrick.Spradlin@cern.ch).

1 Introduction

Measurements of the production cross-sections of charmed mesons in proton-proton collisions test the predictions of quantum chromodynamics (QCD) [1, 2]. Knowledge of open charm production cross-sections is also important for estimating the sensitivity of LHCb for measurements of *CP* violation, mixing, and rare decays of charmed mesons. This note presents a first measurement with the LHCb detector of charm production in pp-collisions at a centre-of-mass energy of 7 TeV. Also presented is a measurement of the ratio of the D^+ to D_s^+ cross-section. Here and throughout this article, references to specific decay modes or specific charmed mesons also imply the charge conjugate mode. The measurements described here are based on $1.81\,\text{nb}^{-1}$ of proton-proton collisions observed with the full LHCb detector [3]. These data were collected in May 2010 under low pile-up conditions with a trigger that accepts events with minimal observable activity in the detector.

Charmed mesons may be produced directly in the pp collision, at the pp collision point from the instantaneous decay of an excited charm resonance, or in the decay of a b-hadron. For this note, the first two sources (direct production and down-feed) are referred to as 'prompt'. Charmed mesons from b-hadron decays are called 'secondary' mesons. The measurements described here are the production cross-sections of prompt charmed mesons. Secondary charmed mesons are treated as backgrounds. No attempt has been made to distinguish between the two sources of prompt charm.

2 Theoretical predictions

Theoretical expectations for the differential cross-sections of prompt D^0, D^+, D^{*+}, and D_s^+ meson production as a function of transverse momentum ($p_{\rm T}$) have been calculated by two groups that we refer to as MC et al. [1] and BAK et al. [2]. Using a spline interpolation of the tabulated values, the predictions have been integrated over bins of $p_{\rm T}$ and rapidity (y) to yield production cross-sections that can be compared directly to the experimental results.

The calculations of MC et al. [1] use the `CTEQ 6.6` parametrisation of the parton densities [4]. They also include estimates of theoretical uncertainties due to the charm quark mass and the renormalisation and factorisation scales. Uncertainties due to the choice of the parton density functions (PDFs) are not included and are expected to be small. Also not included are uncertainties due to higher order QCD effects, which can be estimated by comparing Fixed-Order-Next-to-Leading-Log calculations to predictions from shower Monte Carlo simulations. They are expected to be small in most regions of phase space, but they may become important where the parton shower evolution approaches the soft collinear regime at large y and small $p_{\rm T}$. Hence the theoretical uncertainties may be underestimated. The theoretical calculations assume unit transition probabilities from a primary charm quark to the exclusive hadron state. The actual transition probabilities we used to convert the predictions to measurable cross-sections are those quoted by the PDG [5] based on measurements from e^+e^- colliders close to $\Upsilon(4S)$. The numerical values

are $f(c \to D^0) = 0.565 \pm 0.032$, $f(c \to D^+) = 0.246 \pm 0.020$, $f(c \to D^{*+}) = 0.224 \pm 0.028$, and $f(c \to D_s^+) = 0.080 \pm 0.017$. The uncertainties of these transition probabilities are small in comparison to the other theoretical uncertainties and have not been propagated into the final numbers given below. Note that the transition probabilities do not sum up to unity, since, e.g., $f(c \to D^0)$ has an overlapping contribution from $f(c \to D^{*+})$. Since no dedicated calculation for D_s^+ production was available, the respective prediction was obtained by scaling the D^{*+} prediction by the ratio $f(c \to D_s^+)/f(c \to D^{*+})$. The D^{*+} is kinematically similar to the D_s^+ and also has very little down-feed from higher resonances.

The predictions of BAK et al. [2] are based on the `CTEQ 6.5c0` PDFs [6]. The transition probabilities used in their calculations are given in [7] for $c \to D^0, D^+, D^{*+}$ and in [8] for D_s^+. Only central values for the predictions are currently available.

We also give estimates of the D^0, D^+, D^{*+}, and D_s^+ cross-sections based on PYTHIA [9] with parameter settings adjusted for LHCb [10]. Using Monte Carlo minimum bias events produced with the LHCb full event and detector simulation, we count the number of each species of meson promptly produced in each $p_{\rm T}$ and y bin. Secondary mesons are not included in the count. For each phase space bin, the integrated production cross-section for meson species D, $\sigma(D)$, is calculated from the meson count, $N(D)$, by $\sigma(D) = \sigma_{\rm tot} N(D)/N_{\rm tot}$ where $N_{\rm tot}$ is the number of proton-proton collisions in the generated events and $\sigma_{\rm tot} = (91.05 \pm 0.06)\,{\rm mb}$ is the total proton-proton interaction cross-section given by the LHCb tuning of PYTHIA. The uncertainties quoted for these estimates are statistical uncertainties combining a binomial error for $N(D)/N_{\rm tot}$ and the statistical uncertainty of $\sigma_{\rm tot}$.

The numerical values for the theoretical predictions are collected in Appendix A. In all cases, the numbers correspond to the sum of the cross-sections over the charge conjugate states. A graphical representation of the theoretical predictions is given below together with the experimental results in Sect. 4 (Figs. 5–8). The theoretical uncertainties shown there are for the predictions by MC et al. [1]. However, as they show the effect of scale dependence and uncertainties in the charm quark mass, they can be expected to apply to the other predictions as well. As those uncertainties refer to global parameters of the calculation, they are fully correlated among all bins.

3 Analysis strategy

The analysis is based on fully reconstructed decays of D^0, D^+, D^{*+}, and D_s^+ mesons in the following decay modes:

- D^0: $D^0 \to K^-\pi^+$,
- D^+: $D^+ \to K^-\pi^+\pi^+$,
- D^{*+}: $D^{*+} \to \pi^+ D^0 (K^-\pi^+)$,
- $D_{(s)}^+$: $D^+ \to \phi(K^-K^+)\pi^+$ or $D_s^+ \to \phi(K^-K^+)\pi^+$.

Note that $D^+_{(s)}$ always refers to the both the D^+ and the D^+_s decay into the $\phi(K^+K^-)\pi^+$ final state. The last two modes are used in the measurement of the cross-section ratio $\sigma(D^+)/\sigma(D^+_s)$.

Comparisons with the predictions of QCD are facilitated by performing our measurements in two-dimensional bins of $p_{\rm T}$ and y of the reconstructed meson. For our comparisons of D^0, D^+, and D^{*+}, we use eight bins of width $1\,{\rm GeV}/c$ in the range $0 < p_{\rm T} < 8\,{\rm GeV}/c$, and five bins of width 0.5 units in the range $2 < y < 4.5$. For comparisons of D^+_s, we use two binnings: either eight $p_{\rm T}$ bins of width $1\,{\rm GeV}/c$ and a single y bin spanning $2 < y < 4.5$ or five y bins of 0.5 unit width and a single $p_{\rm T}$ bin spanning $0 < p_{\rm T} < 8\,{\rm GeV}/c$.

The ratio $\sigma(D^+)/\sigma(D^+_s)$ was first presented at ICHEP 2010 and the absolutely normalised cross-sections for D meson production at CKM 2010. Earlier preliminary cross-section results expressed as ratios to theory without absolute normalisation [11] are superseded by those shown in the present note.

3.1 Selection criteria

The selection criteria for each decay mode were tuned independently, with the exception of the decay $D^+ \to \phi(K^-K^+)\pi^+$ for which we use the $D^+_s \to \phi(K^-K^+)\pi^+$selection. Table 1 shows the complete set of criteria for all modes. Each track used in the reconstruction must satisfy the basic quality criterion of an upper limit on the χ^2 per degree of freedom of the track fit. Because D^0, D^+, and D^+_s mesons travel before decaying, the trajectories of their decay products will not, in general, point directly back to the primary interaction vertex (PV) at which the D meson was produced. To exploit this feature, each final state candidate used to reconstruct a D^0, D^+, or D^+_s is required to have a minimum impact parameter (IP) χ^2 with respect the PV. For D^0 reconstruction, a single lower limit is used for each final state particle. Three body decays of D^+ and D^+_s are more efficiently reconstructed by using a relatively small lower limit for all final state particles but larger thresholds for one or two of them. As a result of their production mechanism, final state decay products of charmed mesons have transverse momenta that are generally larger than those of similar particles produced at the PV. Cuts on the $p_{\rm T}$ of the final state tracks were found to be useful in suppressing combinatoric backgrounds in D^0 and $D^+(K\pi\pi)$. As a last criterion for the final state particles, we require that each final state kaon or pion in D^0, D^+, and D^+_s candidates is positively identified by LHCb's particle identification (PID) system. The LHCb PID algorithms assign likelihoods that individual charged tracks were produced by the passage of pions, kaons, protons, muons, and electrons through the detector. For kaons we require that the logarithm of the ratio of kaon to pion likelihoods ($\log(\mathcal{L}_K/\mathcal{L}_\pi)$) exceeds an optimised lower limit. Similarly, pions are required to have a value of $\log(\mathcal{L}_K/\mathcal{L}_\pi)$ that falls below an upper limit.

We consider each appropriate combination of the selected final state particles as a candidate D meson decay and apply additional criteria to select true D mesons produced in the PV. Candidate $D^+_{(s)} \to \phi(K^-K^+)\pi^+$ decays are reconstructed as $D^+_{(s)} \to K^-K^+\pi^+$ decays with the added requirement that the invariant mass of the K^-K^+ combination

Table 1: Selection criteria for $D^0/D^{*+}/D^+_{(s)}$ candidates. h denotes a pion or kaon product of a $D^0/D^+_{(s)}$ decay. The D^{*+} column includes the selection criteria used for D^0 candidates used in the D^{*+} reconstruction, which differ slightly from the D^0 selection used in the measurement of D^0 cross-sections. Where multiple values are listed for selection criteria of the kaon or pion products of a D^+ decay ($IP\chi^2$ and $p_{\rm T}$), all of the final state candidates are required to pass the least restrictive requirement, at least two of the three are required to pass the middle requirement, and at least one of the three is required to pass the most restrictive requirement. For the $D^+_{(s)}(\phi\pi)$ selection sufficient background rejection is already achieved by asking a large $IP\chi^2$ only for the final state pion.

	Variable name	D^0	D^{*+}	$D^+(K\pi\pi)$	$D^+_{(s)}(\phi\pi)$
$h^\pm$	track $\chi^2/N_{\rm dof}<$	9	10	10	4
	$IP\ \chi^2>$	9	9	$3, 10, 50$	$2(K), 10(\pi)$
	$p_{\rm T}({\rm MeV}/c)>$	700		$200, 400, 400$	
	$\lvert\vec{p}\rvert({\rm GeV}/c)>$	5		3.2	
$K^\pm$	$\log(\mathcal{L}_K/\mathcal{L}_\pi)>$	0	0	6	9
$\pi^\pm$	$\log(\mathcal{L}_K/\mathcal{L}_\pi)<$	0	0	6	-2
$\phi(KK)$	$m(KK)({\rm GeV}/c^2)\in$				$(1, 1.04)$
$D^0/D^+_{(s)}$	vertex $\chi^2/N_{\rm dof}<$	9	9	2.67	5
	$FD\ \chi^2>$	16		90	67
	τ(ps)		>0.3	<10	
	proper time $\chi^2<$	9	9		
	$\cos(\theta)>$	0.99993		0.9999	0.9999
	$\cos(\theta_\pi)<$		0.9		
D^{*+}	vertex $\chi^2/N_{\rm dof}<$		16		

falls within a $\pm 20\,{\rm MeV}/c$ window around the $\phi(1020)$ mass. We determine a best-fit common vertex of the final state particles for each candidate D^0, D^+, or D^+_s and require that the χ^2 per degree of freedom for the vertex fit falls below an upper limit. The flight distance of true D^0, D^+, and D^+_s mesons is exploited by requiring that the fitted decay vertex is displaced from the PV, either with a lower limit cut on the measured lifetime (D^0 candidates used in D^{*+} reconstruction) or on the χ^2 between the fitted decay vertex and the PV (all other decay modes). The trajectory of a true prompt D meson should point back to the PV in which it was produced. We make two kinds of pointing criteria to select D meson candidates consistent with origination from a PV. The first, applied to all D^0 candidates, is that the extrapolated trajectories must have an $IP\chi^2$ less than 9. The second kind of criterion, used in the selections for D^+, D^+_s, and D^0 without D^{*+}, is that the D momentum is aligned with the displacement from the PV to its decay vertex. This criterion is applied as a lower limit on the cosine of the angle between these vectors ($\cos(\theta)$). A last variable, used only in the selection of D^0 decays for D^{*+} reconstruction, is the angle between the momentum of the pion from the candidate D^0 evaluated in the

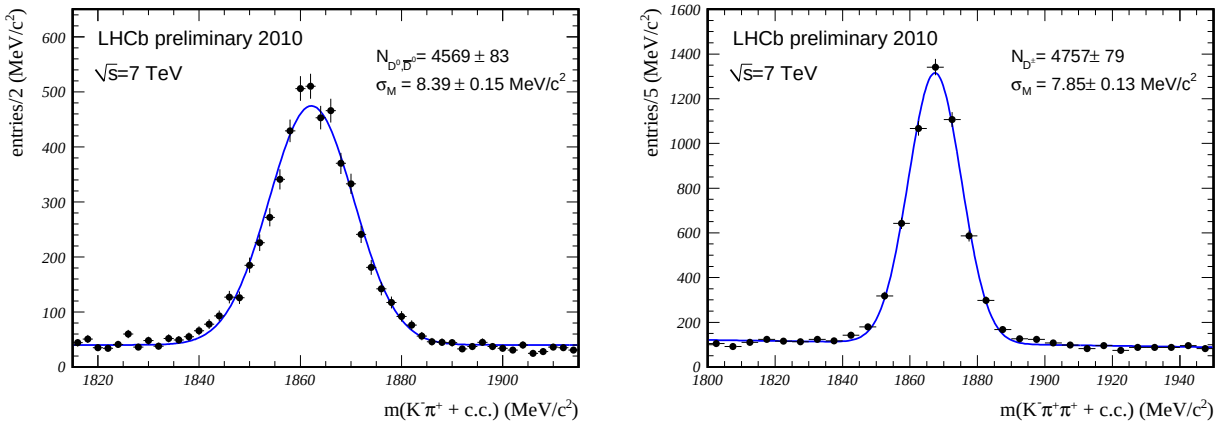

Figure 1: Reconstructed D^0 (left) and D^+ (right) mass peaks. The D^0 was reconstructed in the channel $D^0 \to K\pi$, the D^+ in the mode $D^+ \to K\pi\pi$. The signals are the sums over the charge conjugate states. The curves are the results of fits assuming Gaussian peaks on a constant (D^0) and linear (D^+) background, respectively.

D^0 rest frame and the momentum of the D^0 in the laboratory frame. The cosine of this angle ($\cos\theta_\pi$) has a flat distribution for true D^0 decays but peaks strongly in the forward direction for combinatoric backgrounds. D^{*+} candidates are reconstructed from D^0 candidates and an additional 'slow' pion, which is required to satisfy the same track fit $\chi^2/N_{\rm dof}$ criteria applied to the D^0 daughters. We fit for a common vertex of the slow pion and extrapolated D^0 candidate trajectory and require that the $\chi^2/N_{\rm dof}$ of this D^{*+} decay vertex fit is less than 16. Figures 1–3 show the invariant mass distributions of the selected D candidates in data.

3.2 Yield extraction

Yields of D meson decays are measured independently for each decay mode in each bin of $p_{\rm T}$ and y with fits to the reconstructed D meson invariant mass distributions. These yields are the sum of prompt and secondary mesons. As illustrated by Fig. 4, we use the distribution of the IP of the D meson with respect to the PV to discriminate between prompt and secondary sources of true D mesons. A fit to the background subtracted distributions allows the statistical disentanglement of prompt and non-prompt components. The selection criteria used in the analyses strongly suppress the secondary component. This does not leave enough information to estimate the secondary component in each $(p_{\rm T}, y)$ bin independently, so the fractions of secondary yields are estimated from the full data set and applied uniformly for all bins. Monte Carlo simulations were used to check the procedure and to determine corrections for variations of the non-prompt background over the accessible phase space.

Efficiencies of the selections are determined for each $(p_{\rm T}, y)$ bin with a combination of MC studies and independent studies in data. For each selection, the efficiency of the pion and kaon PID likelihood ratio criteria, $\epsilon_{\rm PID}$, is factored out of the total efficiency

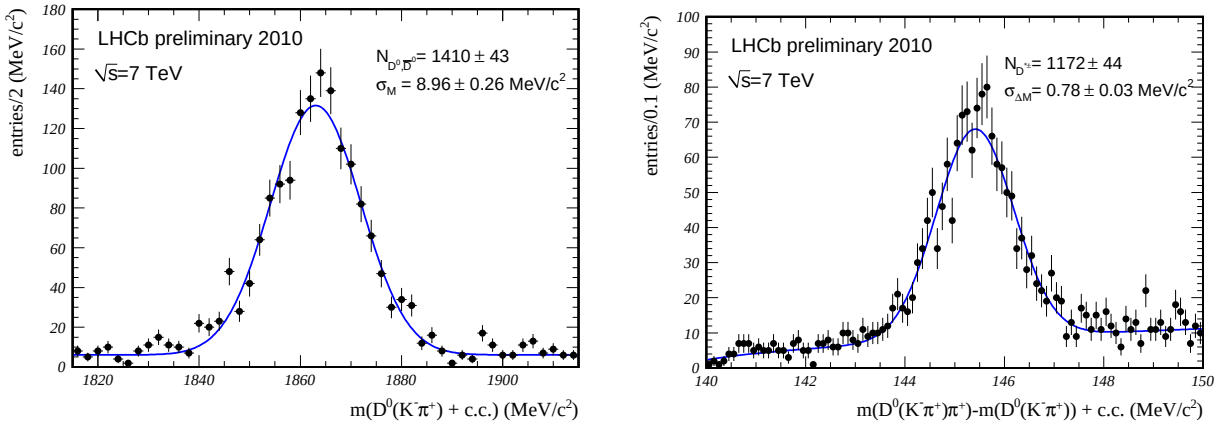

Figure 2: Extraction of the D^{*+} signal in the decay channel $D^{*+} \to D^0\pi^+$. The left hand plot shows the D^0 signal within the D^{*+} combinations, the right hand one is the spectrum of the mass difference between the D^{*+} candidates and the D^0 candidate. The D^0 yield is larger than the D^{*+} yield due to the presence of random slow pion backgrounds in which prompt D^0 mesons combine with random pions from the event to form fake D^{*+} candidates. Such candidates contribute to the D^0 yield but appear as a non-peaking backgrounds in the mass difference plot. The spectra are the sums over charge conjugate states. The fitted curves are Gaussian peaks on top of a linear background for the D^0 mass spectrum (left) or a threshold function proportional to $\sqrt{(m-m_\pi)}$ for the mass difference (right).

and evaluated independently. The PID efficiencies for final state particles are measured in data in bins of track $p_{\rm T}$ and pseudorapidity, η, using high purity samples of pions and kaons from K^0_S, $\phi(1020)$, and Λ^0 hadrons. The effective PID efficiency for each D $(p_{\rm T}, y)$ bin is determined by calculating the average D efficiency over the bin using these final state PID efficiencies and the final state $(p_{\rm T}, \eta)$ distributions from MC simulated decays. The efficiencies of the remaining selection criteria are determined from MC studies, with the exception of the track fit χ^2 confidence level and vertex fit $\chi^2/N_{\rm dof}$ used in the D^+ selection, which are measured in data.

3.3 Systematic uncertainties

Sources of systematic uncertainty can be divided into correlated uncertainties that apply equally to all $(p_{\rm T}, y)$ bins and uncorrelated sources that are evaluated independently for each bin. The correlated uncertainties include contributions that affect the overall normalisation of the cross-sections but that are irrelevant for the measurements of the D^+ to D^+_s ratios. These include the uncertainty in the measurement of luminosity and the overall uncertainty in the tracking efficiency. Systematic uncertainties related to peaking backgrounds caused by cloned tracks in multiple candidate events are estimated from MC and also included as correlated systematic errors.

The branching fractions entering in the analysis are summarised in Tab. 2. Uncertain-

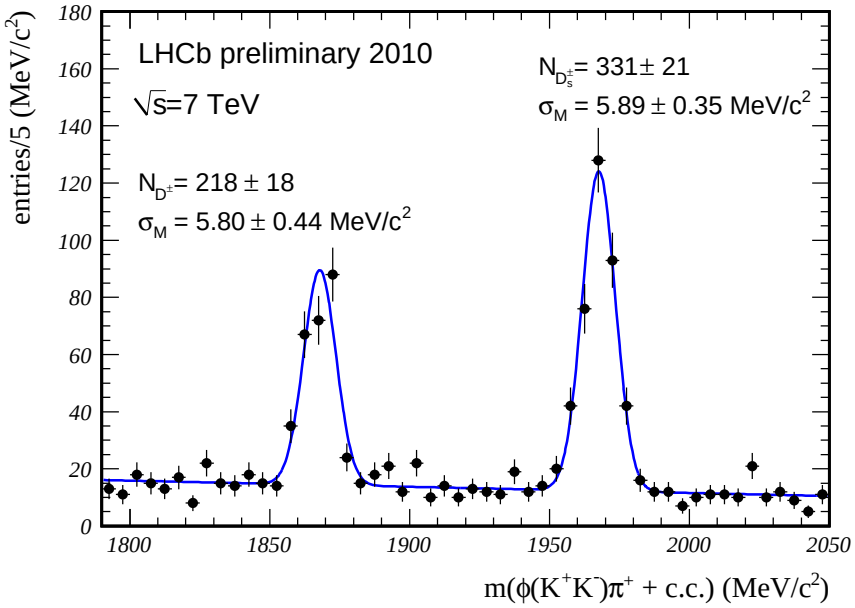

Figure 3: Reconstructed D_s^+ and D^+ mass peaks in the channels $D_s^+ \to \phi(K^-K^+)\pi^+$ and $D^+ \to \phi(K^-K^+)\pi^+$. Shown are the sums over the charge conjugate modes. The curve is the result of a fitting a sum of two Gaussians on top of a linear background.

ties in the branching fraction ratios are propagated into the systematic uncertainties of the final cross-sections and the ratio of D^+ to D_s^+, where both are reconstructed in the $D_{(s)}^+ \to \phi(K^-K^+)\pi^+$ decay mode.

Table 2: Branching fractions of selected hadronic decay modes. The branching fraction shown for $D^{*+} \to \pi^+ D^0(K^-\pi^+)$ is the product of the branching fractions for $D^0 \to K^-\pi^+$ and $D^{*+} \to \pi^+ D^0$ assuming uncorrelated uncertainties.

Decay	Branching fraction	reference
$D^0 \to K^-\pi^+$	$(3.91 \pm 0.05)\%$	[12]
$D^+ \to K^-\pi^+\pi^+$	$(9.29 \pm 0.25)\%$	[12]
$D^+ \to \phi(K^-K^+)\pi^+$	$(0.306 \pm 0.034)\%$	[12]
$D^{*+} \to \pi^+ D^0$	$(67.7 \pm 0.5)\%$	[12]
$D^{*+} \to \pi^+ D^0(K^-\pi^+)$	$(2.65 \pm 0.04)\%$	[12]
$D_s^+ \to \phi(K^-K^+)\pi^+$	$(2.24 \pm 0.13)\%$	[13]

Uncorrelated sources of systematic uncertainty are evaluated in each $(p_{\rm T}, y)$ bin. These include uncertainties of the selection efficiencies due to data-MC differences in distributions of selection variables (typically 2–8%), uncertainties in the yield extraction fit (1–4.5%), uncertainties in the prompt-secondary discrimination (1–4%), the statistical uncertainties of the PID efficiencies calculated from data (1–4%), and the statistical uncertainties of the selection efficiencies determined from MC (MC statistics, 1–2%). In the

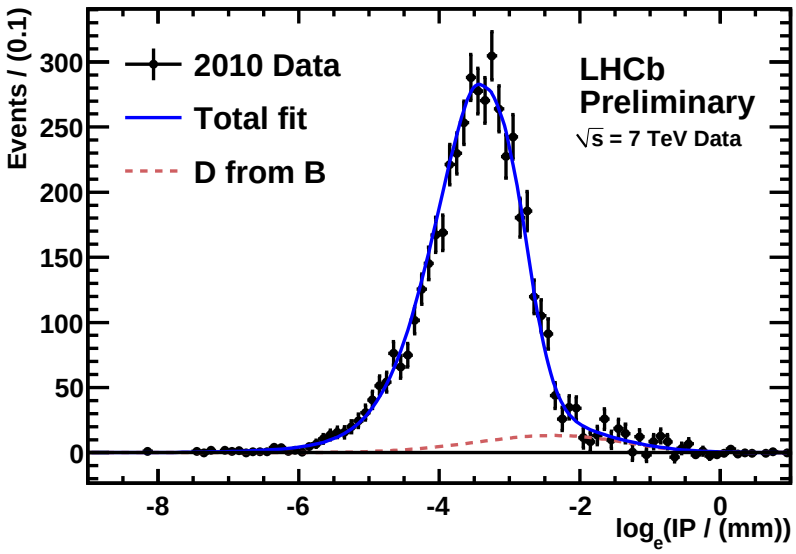

Figure 4: Distribution of the logarithm of the D^+ meson impact parameters at the primary vertex. The data are described by by the sum of a dominant prompt component and a small contribution due to D^+ mesons from B-decays, which show up as a tail at large impact parameters. The curves are a bifurcated Gaussian for the prompt component and a single Gaussian for D mesons from long lived particles.

measurement of the ratio of D^+ to D_s^+ cross-sections, both mesons are reconstructed in the $D^+_{(s)} \to \phi(K^-K^+)\pi^+$ decay mode with the same selection criteria resulting in the cancellation of many of the components of the selection efficiency systematic uncertainties, including the PID efficiency systematics. Non-resonant contributions to the decay modes with an intermediate ϕ-state are small and have been neglected in the current analysis.

4 Cross-section measurements

The signal yields extracted from the data allow us to measure the cross-section as a function of transverse momentum and rapidity in the range $0 < p_{\rm T} < 8\,{\rm GeV}/c$ and $2 < y < 4.5$. The cross-section, σ, measured in bins of those variables are calculated by using the relation

$$\sigma = \frac{N_{\rm signal}}{\varepsilon_{\rm tot} \cdot {\rm BF} \cdot L_{\rm int}},$$

where N_{signal} is the bare signal yield in a given $(y, p_{\rm T})$ bin, $\varepsilon_{\rm tot}$ is the total efficiency for measuring the signal decay in the bin (including acceptance, reconstruction, selection, and trigger), BF is the branching fraction of the particular decay, and $L_{\rm int}$ is the total integrated luminosity.

The numerical values of the measured cross-sections are given in Appendix B, together with a breakdown of the errors in statistical and systematic uncertainties. In the tables

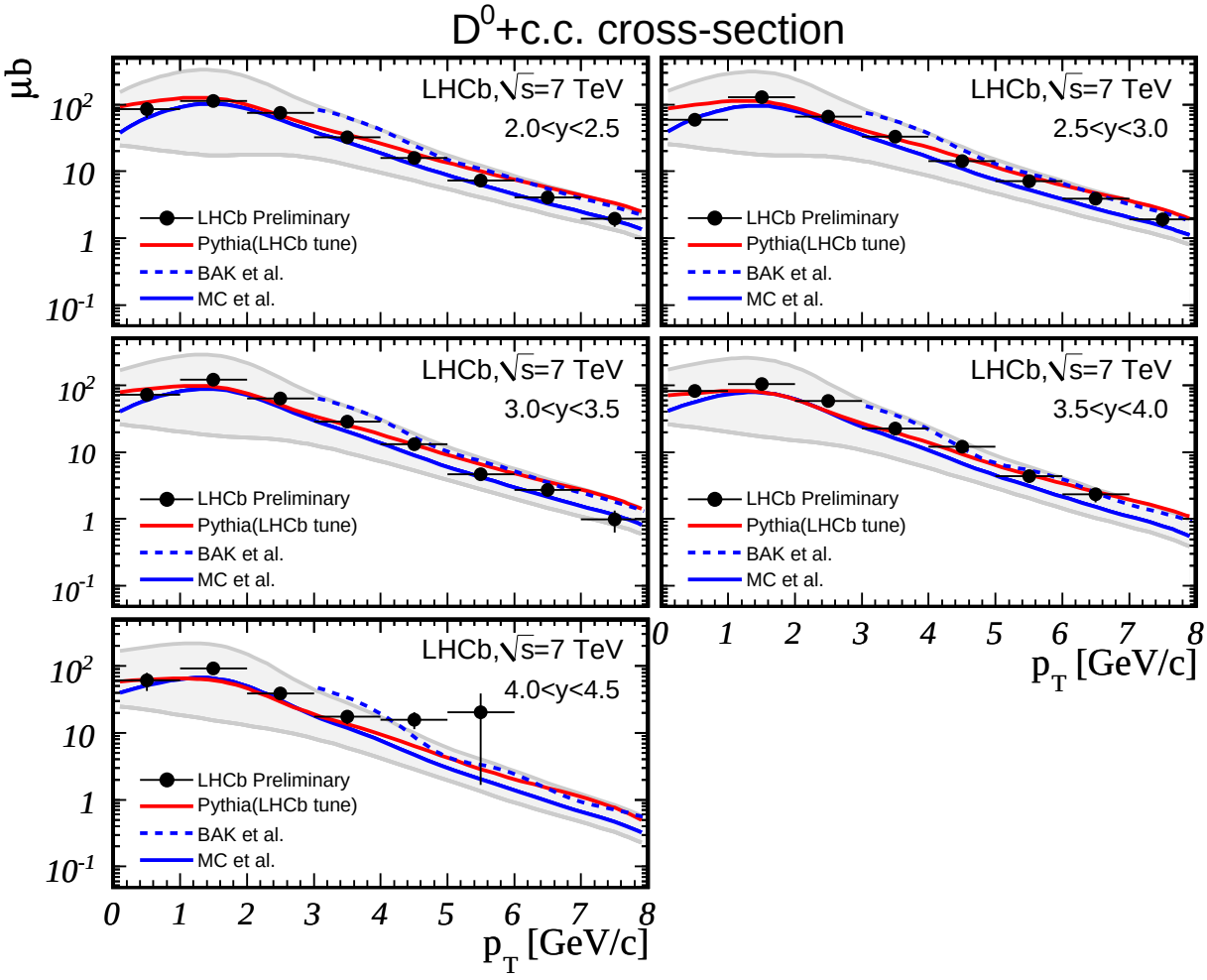

Figure 5: Measured D^0 cross-sections compared to theoretical prediction. Data are shown as a function of $p_{\rm T}$ for different ranges in y. The error bars show statistical and uncorrelated systematics added in quadrature. In addition, there is a global correlated error of 12%. The shaded areas are theoretical uncertainties of the predictions by MC et al. [1].

only the uncorrelated contributions are given. Errors that are correlated between all bins, such as uncertainties of the luminosity, tracking efficiencies, or branching ratios, are quoted in the captions.

The measured cross-sections compared to the theoretical predictions are shown in Figs. 5–8. Only measurements with a total uncorrelated error below 100% are shown. For better visibility, theoretical predictions are displayed as smooth curves such that the value at the bin centre corresponds to the cross-section calculated in that bin. The data points with their uncertainties, which are always drawn at the bin centre, thus can be directly compared with theory. Curves are shown for MC et al. [1], BAK et al. [2], and the LHCb tune of PYTHIA [10]. Experimental uncertainties are the statistical and uncorrelated systematic errors added in quadrature. Common systematics are quoted in the figure

captions. Theoretical uncertainties are only shown for the prediction by MC et al. [1].

Figure 9 shows the measured cross-section ratios $\sigma(D^+)/\sigma(D_s^+)$ integrated over $2.0 < y < 4.5$ as a function of $p_{\rm T}$. Within the uncertainties of the measurement, no $p_{\rm T}$-dependence is observed. Fitting a constant to the distribution gives the value $2.32 \pm 0.27(\text{stat}) \pm 0.26(\text{syst})$. To leading order, this is a measurement of the ratio of the transition probabilities $f(c \to D^+)/f(c \to D_s^+)$. The measured value is consistent with the expectation 3.08 ± 0.70 based on the values quoted in reference [5] with a significantly reduced error.

Measurements and predictions generally are in good agreement. The data points tend to be a bit higher than the expectations from PYTHIA [10], but agree within errors for most of the accessible phase space. One also observes that the QCD calculations [1] and [2] tend to bracket the data, i.e., the current understanding of the dynamics of charm production at LHC energies is consistent with the experimental results. It is interesting to note that this holds for the calculations performed at the natural values for renormalisation and factorisation scale, which suggests that higher order QCD corrections are small.

5 Integrated cross-sections

The cross-sections for D^0, D^{*+}, D^+, and D_s^+ presented above have been integrated over the accessible phase space $0 < p_{\rm T} < 8\,\text{GeV}/c$ and $2 < y < 4.5$, taking into account all bins with non-zero cross-section and less than 100% bin-by-bin error. The extrapolation to the full LHCb phase space is based on the LHCb tune of PYTHIA [10].

The global systematic uncertainties for the individual measurements are collected in Tab. 3. They cover systematic uncertainties from luminosity, tracking efficiency, extrapolation errors, branching ratios and multiple candidates caused by clone tracks. The first three contributions are assumed to be correlated between different analyses, and the others are taken as uncorrelated. All errors are given in percent.

The extrapolation to the full LHCb phase space relies on a model-dependent factor estimated from LHCb MC. Ideally, the systematic uncertainty associated with it should be assessed from the scatter of results obtained from an ensemble of different models. Here, only a single model is available, so a different approach has to be chosen. If the extrapolation factor deviates from unity, then the only scale that can be used to assess its uncertainty is the deviation from one. Here it is assumed that the chosen model is typical, but that alternative models with uniform probability could predict any factor in a range of $\pm 50\%$ of the actual deviation from unity. The RMS of this assumed distribution of extrapolation factors is taken as the systematic uncertainty. This extrapolation error comes on top of the global systematic uncertainties previously discussed for the differential measurements.

Taking all uncertainties into account, the integrated cross-sections over the LHCb

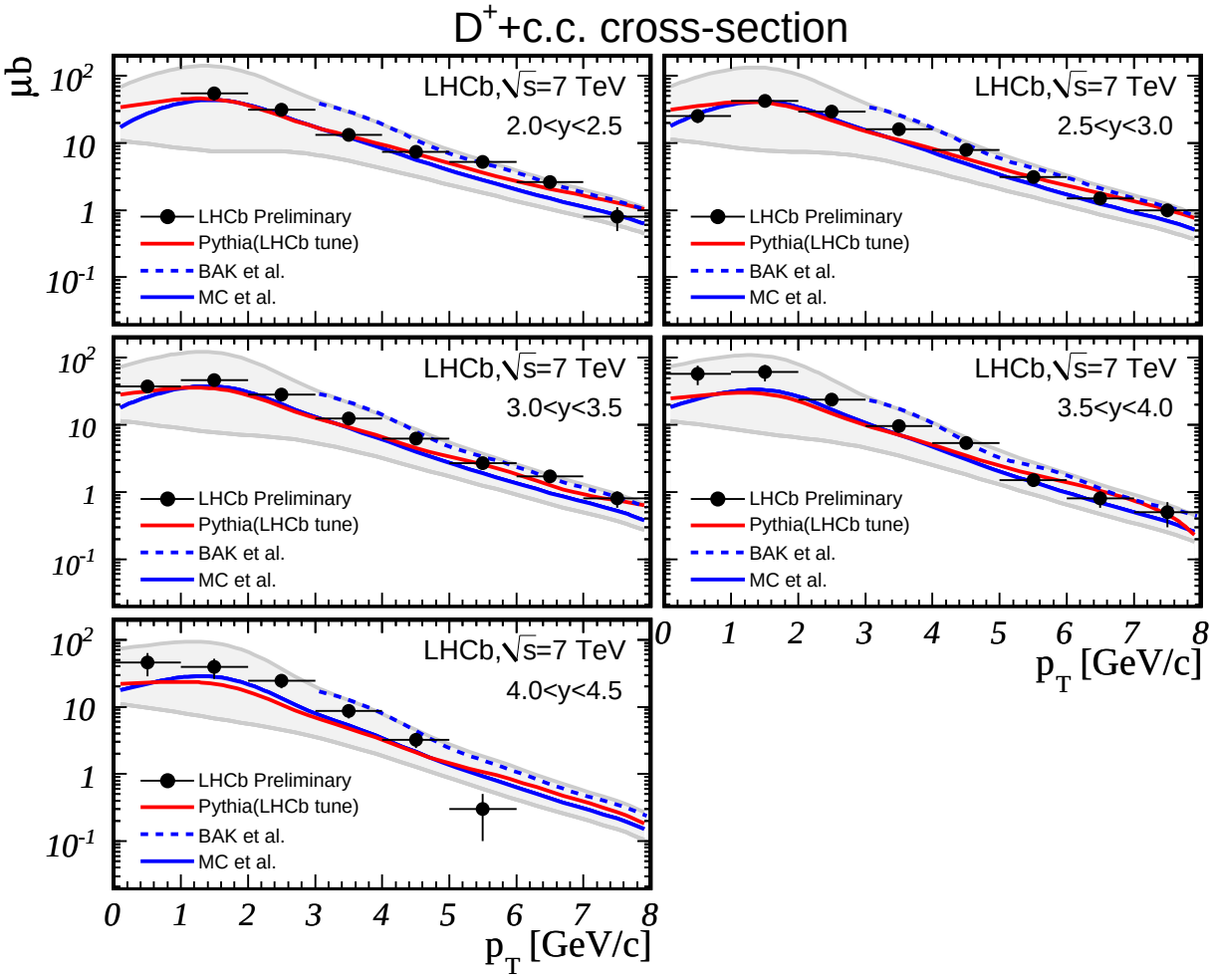

Figure 6: Measured D^+ cross-sections compared to theoretical prediction. Data are shown as a function of $p_{\rm T}$ for different ranges in y. The error bars show statistical and uncorrelated systematics added in quadrature. In addition, there is a global correlated error of 14%. The shaded areas are theoretical uncertainties of the predictions by MC et al. [1].

acceptance become

$$\begin{aligned}
\sigma(D^0) &= 1488 \pm 41 \pm 34 \pm 174\,\mu\text{b} = 1488 \pm 182\,\mu\text{b},\\
\sigma(D^{*+}) &= 676 \pm 64 \pm 21 \pm 119\,\mu\text{b} = 676 \pm 137\,\mu\text{b},\\
\sigma(D^+) &= 717 \pm 39 \pm 26 \pm 98\,\mu\text{b} = 717 \pm 109\,\mu\text{b},\\
\sigma(D_s^+) &= 194 \pm 23 \pm 16 \pm 26\,\mu\text{b} = 194 \pm 38\,\mu\text{b}.
\end{aligned}$$

For comparison, the predictions by PYTHIA [10] are $\sigma(D^0) = 1402 \pm 2\,\mu$b, $\sigma(D^{*+}) = 653 \pm 1\,\mu$b, $\sigma(D^+) = 509 \pm 1\,\mu$b and $\sigma(D_s^+) = 255 \pm 1\,\mu$b. The errors are the statistical errors, uncorrelated systematics, and systematics that are assumed to be 100% correlated between different measurements. The variances of the measurements (diagonal terms of the covariance matrix) are given by the squares of the total errors and the covariances

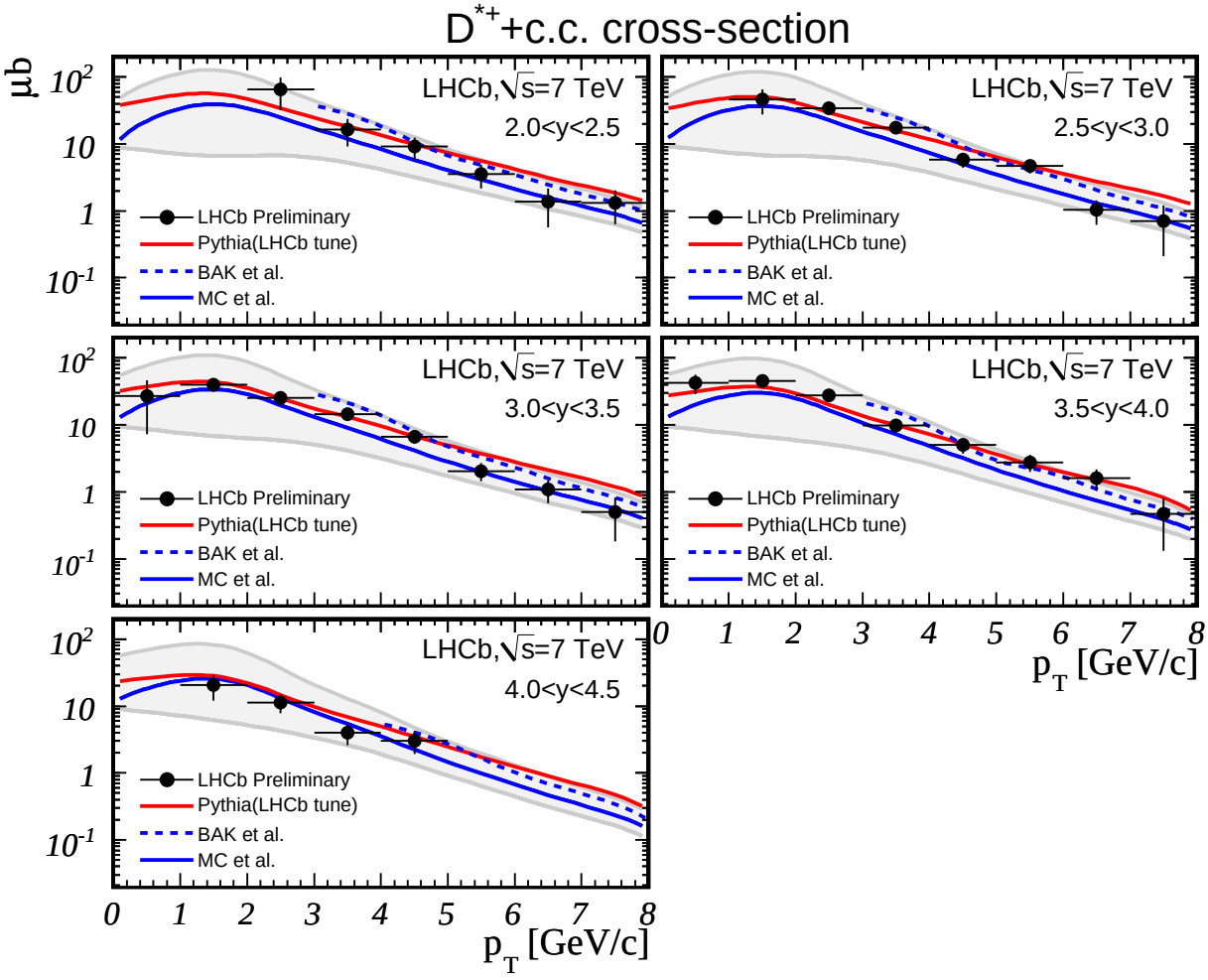

Figure 7: Measured D^{*+} cross-sections compared to theoretical prediction. Data are shown as a function of $p_{\rm T}$ for different ranges in y. The error bars show statistical and uncorrelated systematics added in quadrature. In addition, there is a global correlated error of 14%. The shaded areas are theoretical uncertainties of the predictions by MC et al. [1].

(off-diagonal terms) by the products of the correlated errors. This allows calculation of cross-section ratios with proper treatment of the correlations. Standard error propagation then gives the following results:

$$\frac{\sigma(D^0)}{\sigma(D^{*+})} = 2.20 \pm 0.48, \qquad \frac{\sigma(D^0)}{\sigma(D^+)} = 2.07 \pm 0.37, \qquad \frac{\sigma(D^0)}{\sigma(D_s^+)} = 7.67 \pm 1.67,$$
$$\frac{\sigma(D^{*+})}{\sigma(D^+)} = 0.94 \pm 0.22, \qquad \frac{\sigma(D^{*+})}{\sigma(D_s^+)} = 3.48 \pm 0.93, \qquad \frac{\sigma(D^+)}{\sigma(D_s^+)} = 3.70 \pm 0.84.$$

Using the transition probabilities $f(c \to H)$ from a charm quark into a hadron H, the above cross-sections for specific hadrons can be translated into $c\bar{c}$ production cross-

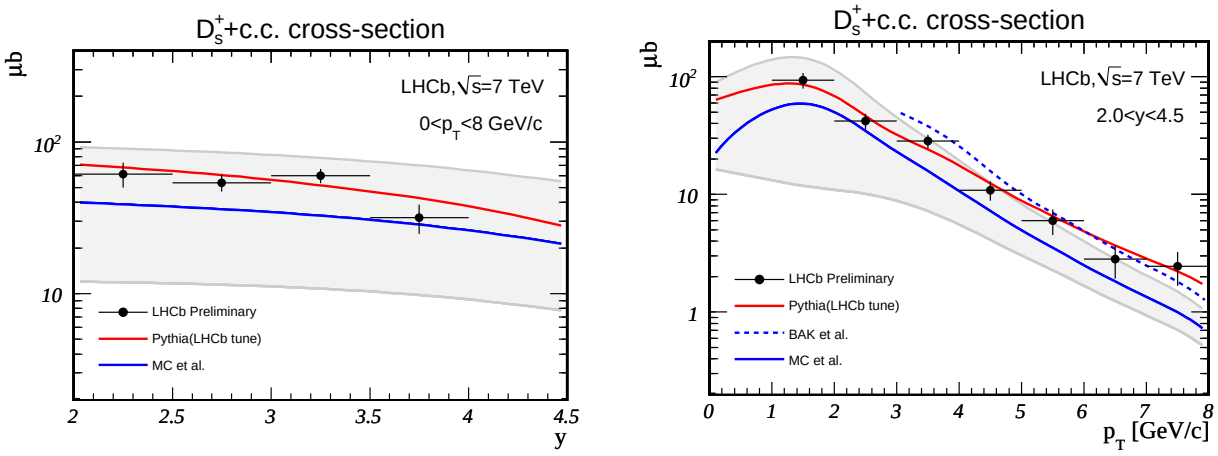

Figure 8: Measured D_s^+ cross-sections compared to theoretical prediction. Data are shown as a function of y integrated over $0 < p_{\rm T} < 8\,{\rm GeV}/c$ (left) and as a function of $p_{\rm T}$ integrated over $2 < y < 4.5$ (right). Measurements with an uncertainty larger than 100% are not shown. The error bars show statistical and uncorrelated systematics added in quadrature. In addition, there is a global correlated error of 16%. The shaded areas are theoretical uncertainties of the predictions by MC et al. [1].

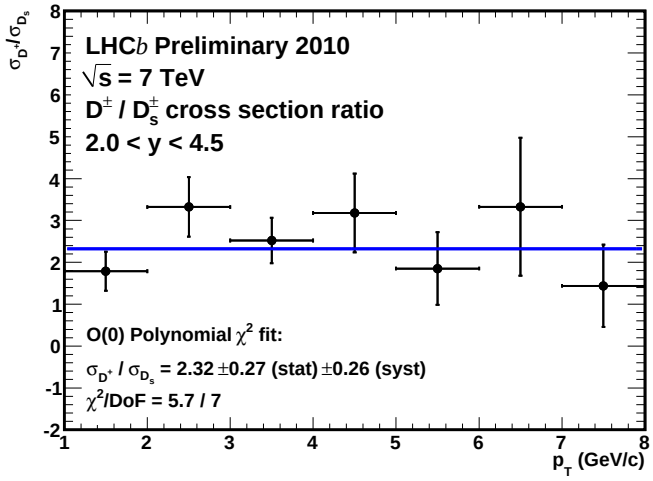

Figure 9: Measured cross-section ratio $\sigma(D^+ + c.c)/\sigma(D_s^+ + c.c.)$. The measurements are integrated over rapidity in the range $2.0 < y < 4.5$. The line shows the average value obtained by fitting a constant to the data points.

sections. Since primary quarks are always produced in pairs, it follows that $\sigma(c\bar{c}) = \sigma(D+\bar{D})/(2f(c \to D)) = C \cdot \sigma(D+\bar{D})$. Numerical values for the transition probabilities can be found in the literature [5,7,8]. A compilation is given in Tab. 4. Values are quoted either for an energy scale in the Υ region or at the Z mass.

A priori, it is not obvious which energy scale is the relevant one for the LHCb mea-

Table 3: Global systematic uncertainties of the individual analyses. All numbers are given in percent. The errors on the branching ratios are taken from [12]. Correlated contributions are assumed to be 100% correlated between different analyses.

	D^0	D^{*+}	D^+	D_s^+
luminosity	10.0	10.0	10.0	10.0
tracking efficiency	6.0	10.0	9.0	9.0
extrapolation	0.1	10.4	2.5	
total correlated	11.7	17.6	13.7	13.5
branching ratio	1.3	1.5	2.7	8.0
multiple candidates			1.0	
total uncorrelated	1.3	1.5	2.9	8.0
total	11.8	17.7	14.0	15.7

Table 4: Published transition probabilities, f, from a charm quark to a hadron. Columns labelled Υ are quoted for energy scales in the Υ region. Columns labelled M_Z are quoted for energy scales at the Z mass. In fields where two values are quoted, they refer to two distinct fits in the respective publication. The last column contains the conversion factors C from the production cross-sections of distinct charmed mesons to the $c\bar{c}$ cross-section. In absence of error estimates for most of the transition probabilities, the uncertainties of the C values are derived from the range covered by the $1/f$ values in each row.

	Υ [5]	Υ [7]	M_Z [7]	M_Z [8]	C
$c \to D^0$	0.565 ± 0.032	0.522, 0.527	0.591, 0.614	0.658	0.86 ± 0.10
$c \to D^{*+}$	0.224 ± 0.028	0.206, 0.209	0.247 ,0.248	0.259	2.18 ± 0.25
$c \to D^+$	0.246 ± 0.020	0.230, 0.234	0.220, 0.272	0.243	2.06 ± 0.22
$c \to D_s^+$	0.080 ± 0.017			0.100	5.63 ± 0.63

surements. From the initial proton-proton interaction, the M_Z scale appears to be the more natural one. From the p_{T} range covered by the data, the Υ mass scale would be preferred. Therefore, the full ranges of scaling factors covered in Tab. 4 were used for the conversion of the measurements to the $c\bar{c}$-cross-sections. Assuming the uncertainties in the scaling factors to be uncorrelated, the following four production cross-sections are obtained:

$$\begin{aligned}
\sigma(c\bar{c}, D^0) &= 1280 \pm 36 \pm 151 \pm 150\,\mu\mathrm{b} = 1280 \pm 216\,\mu\mathrm{b}, \\
\sigma(c\bar{c}, D^{*+}) &= 1474 \pm 140 \pm 176 \pm 260\,\mu\mathrm{b} = 1474 \pm 343\,\mu\mathrm{b}, \\
\sigma(c\bar{c}, D^+) &= 1474 \pm 80 \pm 164 \pm 202\,\mu\mathrm{b} = 1474 \pm 272\,\mu\mathrm{b}, \\
\sigma(c\bar{c}, D_s^+) &= 1092 \pm 130 \pm 151 \pm 147\,\mu\mathrm{b} = 1092 \pm 247\,\mu\mathrm{b}.
\end{aligned}$$

By coincidence, the D^+ and D^{*+} cross-sections happen to have exactly the same central value. The errors are again split into statistical errors, uncorrelated, and correlated sys-

tematics. To test the consistency of the four values, a combined average is determined by a least-squares fit to a constant, taking into account the correlations between the errors. The result is

$$\sigma(c\bar{c}) = 1234 \pm 189\,\mu\text{b} \quad \text{with} \quad \chi^2/\text{ndf} = 2.28/3\ .$$

Within errors, all four independent measurements are perfectly consistent.

It is interesting to compare these results with measurements of the $b\bar{b}$-production cross-section published in [14]. For this, our $c\bar{c}$-production cross-section measurements have to be extrapolated to the phase space covered in that analysis. The $b\bar{b}$-production analysis reports cross-sections covering two ranges of phase space: one including the pseudorapidity range $2 < \eta < 6$ and the full $p_{\rm T}$ range, $\sigma(b\bar{b})_\eta$, and the other covering the full 4π solid angle and full $p_{\rm T}$ range, $\sigma(b\bar{b})_{4\pi}$. Using PYTHIA, the extrapolation factors from our phase space range $0 < p_{\rm T} < 8\,\text{GeV}/c$ and $2 < y < 4.5$, $\sigma(c\bar{c})_y$, to the two phase spaces reported in [14] have been determined to be $\sigma(c\bar{c})_\eta/\sigma(c\bar{c})_y = 1.412 \pm 0.002$ and $\sigma(c\bar{c})_{4\pi}/\sigma(c\bar{c})_y = 4.943 \pm 0.014$. Applying these extrapolation factors to the combined average $\sigma(c\bar{c})$ above and comparing the results to the measurements reported in [14] gives the following:

$$\begin{aligned} &\sigma(c\bar{c})_y = 1234 \pm 189\,\mu\text{b}, \quad \sigma(c\bar{c})_\eta = 1742 \pm 267\,\mu\text{b}, \qquad \sigma(c\bar{c})_{4\pi} = 6100 \pm 934\,\mu\text{b}, \\ &\qquad\qquad\qquad\quad \sigma(b\bar{b})_\eta = \ 75.3 \pm 14\,\mu\text{b}\ \ [14], \quad \sigma(b\bar{b})_{4\pi} = \ 284 \pm 53\,\mu\text{b}\ \ [14]. \end{aligned}$$

Here the the statistical and systematic errors have been combined in quadrature for the numbers taken from [14]. The cross-sections are the average cross-sections to produce a $c(b)$- or $\bar{c}(\bar{b})$-flavoured hadron within the defined kinematic range. The results show that the charm cross-section at a centre-of-mass energy $\sqrt{s} = 7\,\text{TeV}$ is about 20 times larger than the $b\bar{b}$ production cross-section.

6 Summary

A first measurement of charm production in pp-collisions at a centre-of-mass energy of 7 TeV has been performed with the the LHCb detector, based on an integrated luminosity of $L_{\rm int} = 1.81\,\text{nb}^{-1}$. Cross-section measurements with total uncertainties below 20% have been achieved. The shape and absolute normalisation of the differential cross-sections for $D^0/\overline{D}^0$, $D^{*\pm}$, $D^\pm$, and $D_s^\pm$ mesons is found to be in good agreement with theory predictions and the expectations from the LHCb tune of PYTHIA.

A direct comparison of $D_s^\pm$ and $D^\pm$ production yields a determination of the cross-section ratio $R = \sigma(D^+)/\sigma(D_s^+)$ integrated over $2.0 < y < 4.5$ as a function of $p_{\rm T}$. Within errors the ratio is independent of $p_{\rm T}$. To leading order, the average $R = 2.32 \pm 0.27(\text{stat}) \pm 0.26(\text{syst})$ is a measurement of the ratio of the transition probabilities $f(c \to D^+)/f(c \to D_s^+)$.

The $c\bar{c}$ cross-section for producing a c-flavoured hadron in the range $0 < p_{\rm T} < 8\,\text{GeV}/c$ and $2 < y < 4.5$ is found to be $1.23 \pm 0.19\,\text{mb}$. Using PYTHIA to extrapolate the measurement to full phase space, we find a total cross-section $\sigma(pp \to c\bar{c}X) = 6.10 \pm$

0.93 mb for a proton-proton centre-of-mass energy $\sqrt{s} = 7\,\text{TeV}$, about 20 times the value of the $b\bar{b}$ production cross-section.

A Numerical values of the theoretical predictions

Tables 5–10 show the theoretical predictions for the production cross-sections of charmed mesons.

Table 5: Theoretical predictions for the $D^0 + c.c.$ production cross-section integrated over bins in y and p_{T}. The cross-sections are given in units of μb.

Predictions by MC et al. [1]

p_{T}	y				
(GeV/c)	$(2.0, 2.5)$	$(2.5, 3.0)$	$(3.0, 3.5)$	$(3.5, 4.0)$	$(4.0, 4.5)$
$(0, 1)$	$63\pm^{122}_{41}$	$62\pm^{121}_{39}$	$60\pm^{122}_{36}$	$56\pm^{119}_{33}$	$51\pm^{112}_{29}$
$(1, 2)$	$102\pm^{142}_{84}$	$96\pm^{134}_{78}$	$88\pm^{124}_{70}$	$78\pm^{110}_{60}$	$65\pm^{94}_{50}$
$(2, 3)$	$59\pm^{63}_{41}$	$53\pm^{57}_{37}$	$47\pm^{50}_{32}$	$39\pm^{42}_{26}$	$30\pm^{33}_{20}$
$(3, 4)$	$27\pm^{23}_{15}$	$24\pm^{20}_{13}$	$20\pm^{17}_{10}$	$16\pm^{14}_{8}$	$12\pm^{10}_{6}$
$(4, 5)$	$13\pm^{9}_{5}$	$11\pm^{8}_{5}$	$8.9\pm^{6.4}_{3.6}$	$6.8\pm^{4.9}_{2.7}$	$4.7\pm^{3.5}_{1.8}$
$(5, 6)$	$6.3\pm^{3.8}_{2.2}$	$5.3\pm^{3.2}_{1.8}$	$4.2\pm^{2.6}_{1.4}$	$3.1\pm^{1.9}_{1.0}$	$2.0\pm^{1.3}_{0.7}$
$(6, 7)$	$3.3\pm^{1.8}_{1.0}$	$2.7\pm^{1.5}_{0.8}$	$2.1\pm^{1.2}_{0.7}$	$1.5\pm^{0.8}_{0.5}$	$0.94\pm^{0.53}_{0.30}$
$(7, 8)$	$1.9\pm^{0.9}_{0.5}$	$1.5\pm^{0.7}_{0.4}$	$1.1\pm^{0.6}_{0.3}$	$0.78\pm^{0.39}_{0.23}$	$0.47\pm^{0.24}_{0.14}$

Predictions by BAK et al. [2]

p_{T}	y				
(GeV/c)	$(2.0, 2.5)$	$(2.5, 3.0)$	$(3.0, 3.5)$	$(3.5, 4.0)$	$(4.0, 4.5)$
$(3, 4)$	64	57	48	36	34
$(4, 5)$	24	21	17	12	8.8
$(5, 6)$	11	9.3	7.3	5.4	3.3
$(6, 7)$	5.5	4.6	3.5	2.5	1.5
$(7, 8)$	3.0	2.4	1.8	1.2	0.71

Predictions by PYTHIA [10]

p_{T}	y				
(GeV/c)	$(2.0, 2.5)$	$(2.5, 3.0)$	$(3.0, 3.5)$	$(3.5, 4.0)$	$(4.0, 4.5)$
$(0, 1)$	107.87 ± 0.54	98.80 ± 0.52	88.27 ± 0.49	76.21 ± 0.46	62.18 ± 0.41
$(1, 2)$	124.12 ± 0.58	110.73 ± 0.55	95.28 ± 0.51	79.27 ± 0.47	61.03 ± 0.41
$(2, 3)$	68.44 ± 0.43	60.34 ± 0.41	50.88 ± 0.37	40.38 ± 0.33	29.49 ± 0.28
$(3, 4)$	35.36 ± 0.31	30.82 ± 0.29	25.27 ± 0.26	19.63 ± 0.23	13.50 ± 0.19
$(4, 5)$	18.63 ± 0.22	16.30 ± 0.21	12.99 ± 0.19	9.32 ± 0.16	6.39 ± 0.13
$(5, 6)$	10.04 ± 0.16	8.38 ± 0.15	6.53 ± 0.13	4.60 ± 0.11	2.88 ± 0.09
$(6, 7)$	5.72 ± 0.12	4.77 ± 0.11	3.62 ± 0.10	2.57 ± 0.08	1.50 ± 0.06
$(7, 8)$	3.34 ± 0.09	2.70 ± 0.09	2.00 ± 0.07	1.47 ± 0.06	0.76 ± 0.05

Table 6: Theoretical predictions for the $D^+ + c.c.$ production cross-section integrated over bins in y and $p_{\rm T}$. The cross-sections are given in units of μb.

Predictions by MC et al. [1]

$p_{\rm T}$	y				
(GeV/c)	$(2.0, 2.5)$	$(2.5, 3.0)$	$(3.0, 3.5)$	$(3.5, 4.0)$	$(4.0, 4.5)$
$(0, 1)$	$27\pm^{53}_{18}$	$27\pm^{53}_{17}$	$26\pm^{52}_{16}$	$24\pm^{51}_{14}$	$22\pm^{48}_{13}$
$(1, 2)$	$44\pm^{61}_{36}$	$41\pm^{58}_{33}$	$38\pm^{53}_{30}$	$33\pm^{47}_{26}$	$28\pm^{40}_{21}$
$(2, 3)$	$26\pm^{28}_{18}$	$23\pm^{25}_{16}$	$20\pm^{22}_{14}$	$17\pm^{19}_{11}$	$13\pm^{15}_{9}$
$(3, 4)$	$12\pm^{10}_{7}$	$11\pm^{9}_{6}$	$9.0\pm^{7.8}_{4.7}$	$7.1\pm^{6.3}_{3.7}$	$5.2\pm^{4.7}_{2.6}$
$(4, 5)$	$5.6\pm^{4.1}_{2.5}$	$4.9\pm^{3.5}_{2.1}$	$4.0\pm^{2.9}_{1.7}$	$3.1\pm^{2.3}_{1.2}$	$2.1\pm^{1.6}_{0.8}$
$(5, 6)$	$2.8\pm^{1.7}_{1.0}$	$2.4\pm^{1.5}_{0.8}$	$1.9\pm^{1.2}_{0.7}$	$1.4\pm^{0.9}_{0.5}$	$0.92\pm^{0.60}_{0.32}$
$(6, 7)$	$1.5\pm^{0.8}_{0.5}$	$1.2\pm^{0.7}_{0.4}$	$0.97\pm^{0.53}_{0.30}$	$0.69\pm^{0.39}_{0.22}$	$0.43\pm^{0.25}_{0.14}$
$(7, 8)$	$0.84\pm^{0.41}_{0.24}$	$0.69\pm^{0.34}_{0.20}$	$0.52\pm^{0.26}_{0.15}$	$0.36\pm^{0.18}_{0.11}$	$0.22\pm^{0.11}_{0.07}$

Predictions by BAK et al. [2]

$p_{\rm T}$	y				
(GeV/c)	$(2.0, 2.5)$	$(2.5, 3.0)$	$(3.0, 3.5)$	$(3.5, 4.0)$	$(4.0, 4.5)$
$(3, 4)$	29	26	22	17	13
$(4, 5)$	11	9.7	8.0	5.6	4.4
$(5, 6)$	5.0	4.3	3.4	2.5	1.6
$(6, 7)$	2.5	2.1	1.6	1.1	0.71
$(7, 8)$	1.4	1.1	0.84	0.58	0.35

Predictions by PYTHIA [10]

$p_{\rm T}$	y				
(GeV/c)	$(2.0, 2.5)$	$(2.5, 3.0)$	$(3.0, 3.5)$	$(3.5, 4.0)$	$(4.0, 4.5)$
$(0, 1)$	39.28 ± 0.33	35.54 ± 0.31	31.85 ± 0.29	27.38 ± 0.27	22.89 ± 0.25
$(1, 2)$	44.85 ± 0.35	39.76 ± 0.33	34.80 ± 0.31	28.93 ± 0.28	22.11 ± 0.24
$(2, 3)$	25.01 ± 0.26	21.65 ± 0.24	18.67 ± 0.22	14.81 ± 0.20	10.71 ± 0.17
$(3, 4)$	12.75 ± 0.19	11.17 ± 0.17	9.23 ± 0.16	7.10 ± 0.14	4.78 ± 0.11
$(4, 5)$	6.98 ± 0.14	5.81 ± 0.13	4.57 ± 0.11	3.47 ± 0.10	2.09 ± 0.08
$(5, 6)$	3.64 ± 0.10	3.10 ± 0.09	2.58 ± 0.08	1.83 ± 0.07	1.08 ± 0.05
$(6, 7)$	2.08 ± 0.07	1.77 ± 0.07	1.26 ± 0.06	1.05 ± 0.05	0.55 ± 0.04
$(7, 8)$	1.30 ± 0.06	1.02 ± 0.05	0.75 ± 0.05	0.46 ± 0.04	0.27 ± 0.03

Table 7: Theoretical predictions for the $D^{*+} + c.c.$ production cross-section integrated over bins in y and $p_{\rm T}$. The cross-sections are given in units of μb.

Predictions by MC et al. [1]

$p_{\rm T}$	y				
(GeV/c)	$(2.0, 2.5)$	$(2.5, 3.0)$	$(3.0, 3.5)$	$(3.5, 4.0)$	$(4.0, 4.5)$
$(0, 1)$	$22\pm^{44}_{14}$	$22\pm^{44}_{13}$	$21\pm^{44}_{12}$	$20\pm^{43}_{11}$	$18\pm^{41}_{10}$
$(1, 2)$	$39\pm^{56}_{32}$	$37\pm^{53}_{30}$	$34\pm^{49}_{27}$	$30\pm^{44}_{23}$	$26\pm^{38}_{19}$
$(2, 3)$	$25\pm^{27}_{18}$	$22\pm^{25}_{16}$	$20\pm^{22}_{14}$	$17\pm^{19}_{11}$	$13\pm^{15}_{9}$
$(3, 4)$	$12\pm^{10}_{7}$	$11\pm^{9}_{6}$	$9.0\pm^{8.0}_{4.9}$	$7.2\pm^{6.5}_{3.8}$	$5.4\pm^{4.8}_{2.8}$
$(4, 5)$	$5.7\pm^{4.2}_{2.6}$	$5.0\pm^{3.7}_{2.2}$	$4.1\pm^{3.0}_{1.8}$	$3.2\pm^{2.4}_{1.3}$	$2.2\pm^{1.7}_{0.9}$
$(5, 6)$	$2.9\pm^{1.8}_{1.1}$	$2.5\pm^{1.6}_{0.9}$	$2.0\pm^{1.3}_{0.7}$	$1.5\pm^{0.9}_{0.5}$	$0.98\pm^{0.64}_{0.34}$
$(6, 7)$	$1.6\pm^{0.9}_{0.5}$	$1.3\pm^{0.7}_{0.4}$	$1.0\pm^{0.6}_{0.3}$	$0.73\pm^{0.42}_{0.23}$	$0.46\pm^{0.27}_{0.15}$
$(7, 8)$	$0.88\pm^{0.43}_{0.26}$	$0.73\pm^{0.36}_{0.21}$	$0.56\pm^{0.28}_{0.16}$	$0.38\pm^{0.20}_{0.11}$	$0.23\pm^{0.12}_{0.07}$

Predictions by BAK et al. [2]

$p_{\rm T}$	y				
(GeV/c)	$(2.0, 2.5)$	$(2.5, 3.0)$	$(3.0, 3.5)$	$(3.5, 4.0)$	$(4.0, 4.5)$
$(3, 4)$	28	25	21	16	—
$(4, 5)$	11	9.3	7.9	5.0	4.1
$(5, 6)$	4.8	4.1	3.3	2.3	1.6
$(6, 7)$	2.4	2.0	1.6	1.1	0.69
$(7, 8)$	1.3	1.1	0.83	0.56	0.34

Predictions by PYTHIA [10]

$p_{\rm T}$	y				
(GeV/c)	$(2.0, 2.5)$	$(2.5, 3.0)$	$(3.0, 3.5)$	$(3.5, 4.0)$	$(4.0, 4.5)$
$(0, 1)$	45.61 ± 0.35	41.07 ± 0.33	37.41 ± 0.32	31.81 ± 0.29	26.21 ± 0.27
$(1, 2)$	56.26 ± 0.39	50.30 ± 0.37	43.66 ± 0.34	36.60 ± 0.32	28.18 ± 0.28
$(2, 3)$	34.16 ± 0.30	29.57 ± 0.28	25.11 ± 0.26	20.09 ± 0.23	14.71 ± 0.20
$(3, 4)$	18.31 ± 0.22	15.78 ± 0.21	13.17 ± 0.19	9.97 ± 0.16	6.91 ± 0.14
$(4, 5)$	9.93 ± 0.16	8.66 ± 0.15	6.83 ± 0.14	5.17 ± 0.12	3.49 ± 0.10
$(5, 6)$	5.60 ± 0.12	4.72 ± 0.11	3.73 ± 0.10	2.60 ± 0.08	1.73 ± 0.07
$(6, 7)$	3.13 ± 0.09	2.76 ± 0.09	2.13 ± 0.08	1.54 ± 0.06	0.90 ± 0.05
$(7, 8)$	1.85 ± 0.07	1.66 ± 0.07	1.20 ± 0.06	0.82 ± 0.05	0.47 ± 0.04

Table 8: Theoretical predictions for the $D_s^+ + c.c.$ production cross-section integrated over bins in y and $p_{\rm T}$. The cross-sections are given in units of μb.

Predictions by MC et al. [1]

$p_{\rm T}$	y				
(GeV/c)	$(2.0, 2.5)$	$(2.5, 3.0)$	$(3.0, 3.5)$	$(3.5, 4.0)$	$(4.0, 4.5)$
$(0, 1)$	$7.8\pm^{15.6}_{5.0}$	$7.7\pm^{15.8}_{4.7}$	$7.5\pm^{15.9}_{4.4}$	$7.1\pm^{15.5}_{4.0}$	$6.5\pm^{14.6}_{3.6}$
$(1, 2)$	$14\pm^{20}_{12}$	$13\pm^{19}_{11}$	$12\pm^{18}_{10}$	$11\pm^{16}_{8}$	$9.1\pm^{13.4}_{6.9}$
$(2, 3)$	$8.8\pm^{9.7}_{6.4}$	$8.0\pm^{8.9}_{5.7}$	$7.1\pm^{7.8}_{5.0}$	$5.9\pm^{6.6}_{4.1}$	$4.7\pm^{5.3}_{3.2}$
$(3, 4)$	$4.3\pm^{3.7}_{2.4}$	$3.8\pm^{3.3}_{2.1}$	$3.2\pm^{2.9}_{1.7}$	$2.6\pm^{2.3}_{1.4}$	$1.9\pm^{1.7}_{1.0}$
$(4, 5)$	$2.1\pm^{1.5}_{0.9}$	$1.8\pm^{1.3}_{0.8}$	$1.5\pm^{1.1}_{0.6}$	$1.1\pm^{0.8}_{0.5}$	$0.79\pm^{0.60}_{0.32}$
$(5, 6)$	$1.0\pm^{0.7}_{0.4}$	$0.88\pm^{0.56}_{0.31}$	$0.71\pm^{0.45}_{0.25}$	$0.53\pm^{0.34}_{0.18}$	$0.35\pm^{0.23}_{0.12}$
$(6, 7)$	$0.56\pm^{0.31}_{0.17}$	$0.47\pm^{0.26}_{0.15}$	$0.36\pm^{0.20}_{0.11}$	$0.26\pm^{0.15}_{0.08}$	$0.17\pm^{0.10}_{0.05}$
$(7, 8)$	$0.32\pm^{0.15}_{0.09}$	$0.26\pm^{0.13}_{0.08}$	$0.20\pm^{0.10}_{0.06}$	$0.14\pm^{0.07}_{0.04}$	$0.084\pm^{0.044}_{0.025}$

Predictions by BAK et al. [2]

$p_{\rm T}$	y				
(GeV/c)	$(2.0, 2.5)$	$(2.5, 3.0)$	$(3.0, 3.5)$	$(3.5, 4.0)$	$(4.0, 4.5)$
$(3, 4)$	12	10	8.9	6.9	0.000
$(4, 5)$	4.5	3.9	3.2	2.4	1.7
$(5, 6)$	2.1	1.8	1.4	1.1	0.67
$(6, 7)$	1.1	0.89	0.69	0.50	0.31
$(7, 8)$	0.58	0.48	0.36	0.25	0.15

Predictions by PYTHIA [10]

$p_{\rm T}$	y				
(GeV/c)	$(2.0, 2.5)$	$(2.5, 3.0)$	$(3.0, 3.5)$	$(3.5, 4.0)$	$(4.0, 4.5)$
$(0, 1)$	18.24 ± 0.22	16.82 ± 0.21	15.07 ± 0.20	13.18 ± 0.19	10.87 ± 0.17
$(1, 2)$	22.34 ± 0.25	20.24 ± 0.23	17.45 ± 0.22	14.38 ± 0.20	11.28 ± 0.17
$(2, 3)$	12.56 ± 0.18	11.53 ± 0.18	9.41 ± 0.16	7.45 ± 0.14	5.42 ± 0.12
$(3, 4)$	6.96 ± 0.14	5.69 ± 0.12	4.87 ± 0.11	3.89 ± 0.10	2.69 ± 0.09
$(4, 5)$	3.74 ± 0.10	3.00 ± 0.09	2.50 ± 0.08	1.93 ± 0.07	1.25 ± 0.06
$(5, 6)$	2.04 ± 0.07	1.71 ± 0.07	1.31 ± 0.06	0.89 ± 0.05	0.59 ± 0.04
$(6, 7)$	1.17 ± 0.06	0.97 ± 0.05	0.68 ± 0.04	0.54 ± 0.04	0.32 ± 0.03
$(7, 8)$	0.73 ± 0.04	0.60 ± 0.04	0.44 ± 0.03	0.32 ± 0.03	0.13 ± 0.02

Table 9: Theoretical predictions for the $D_s^+ + c.c.$ production cross-section in bins of $p_{\rm T}$, integrated over $2.0 < y < 4.5$. The cross-sections are given in units of μb.

$p_{\rm T}$	Reference		
(GeV/c)	MC et al. [1]	BAK et al. [2]	PYTHIA [10]
$(0, 1)$	$36\pm^{77}_{22}$	—	74.18 ± 0.44
$(1, 2)$	$59\pm^{86}_{47}$	—	85.69 ± 0.48
$(2, 3)$	$34\pm^{38}_{24}$	—	46.37 ± 0.35
$(3, 4)$	$16\pm^{14}_{9}$	38	24.10 ± 0.25
$(4, 5)$	$7.2\pm^{5.4}_{3.1}$	16	12.42 ± 0.18
$(5, 6)$	$3.5\pm^{2.2}_{1.2}$	7.0	6.54 ± 0.13
$(6, 7)$	$1.8\pm^{1.0}_{0.6}$	3.4	3.68 ± 0.10
$(7, 8)$	$1.0\pm^{0.5}_{0.3}$	1.8	2.22 ± 0.07

Table 10: Theoretical predictions for the $D_s^+ + c.c.$ production cross-section in bins of y, integrated over $(0 < p_{\rm T} < 8)\,{\rm GeV}/c$. The cross-sections are given in units of μb.

y	Reference	
(GeV/c)	MC et al. [1]	PYTHIA [10]
$(2.0, 2.5)$	$39\pm^{52}_{27}$	67.78 ± 0.43
$(2.5, 3.0)$	$36\pm^{49}_{25}$	60.56 ± 0.40
$(3.0, 3.5)$	$33\pm^{46}_{22}$	51.73 ± 0.37
$(3.5, 4.0)$	$28\pm^{42}_{19}$	42.58 ± 0.34
$(4.0, 4.5)$	$24\pm^{36}_{15}$	32.55 ± 0.30

B Measured open charm cross-sections

Tables 11–15 show the numerical values and breakdown of the uncertainties of the cross-section measurements described in the main part of this note.

Table 11: D_s^+ cross-sections in μb as a function of y, integrated over transverse momentum in the range $0 < p_{\mathrm{T}} < 8\,\mathrm{GeV}/c$. The uncertainties given are statistical and uncorrelated systematic uncertainties. Overall correlated relative systematic uncertainties due to tracking (9%), the branching ratio (8%), and luminosity (10%) apply to all bins.

y	Cross-section (μb)
$(2, 2.5)$	$61.4 \pm 11.2 \pm 2.6$
$(2.5, 3)$	$53.8 \pm 6.5 \pm 1.5$
$(3, 3.5)$	$60.0 \pm 6.2 \pm 1.6$
$(3.5, 4)$	$31.7 \pm 6.8 \pm 1.0$
$(4, 4.5)$	—

Table 12: D_s^+ cross-sections in units of μb as a function of p_{T} integrated over the rapidity range $2 < y < 4.5$. The uncertainties given are statistical and uncorrelated systematic uncertainties. Overall correlated relative systematic uncertainties due to tracking (9%), the branching ratio (8%), and luminosity (10%) apply to all bins.

$p_{\mathrm{T}}(\mathrm{GeV}/c)$	Cross-section (μb)
$(0, 1)$	—
$(1, 2)$	$93.6 \pm 14.1 \pm 2.7$
$(2, 3)$	$42.1 \pm 6.2 \pm 1.2$
$(3, 4)$	$28.4 \pm 3.7 \pm 0.9$
$(4, 5)$	$10.9 \pm 2.0 \pm 0.5$
$(5, 6)$	$5.97 \pm 1.43 \pm 0.31$
$(6, 7)$	$2.82 \pm 0.87 \pm 0.17$
$(7, 8)$	$2.46 \pm 0.77 \pm 0.18$

Table 13: D^0 cross-sections in μb in bins of $p_{\rm T}$ and y. The uncertainties given are statistical and uncorrelated systematic uncertainties. Overall correlated relative systematic uncertainties due to tracking (6%), the branching ratio (1.3%), and luminosity (10%) apply to all bins.

$p_{\rm T}$	y				
(GeV/c)	$(2.0, 2.5)$	$(2.5, 3.0)$	$(3.0, 3.5)$	$(3.5, 4.0)$	$(4.0, 4.5)$
$(0, 1)$	$85.6 \pm 21.6 \pm 5.1$	$58.8 \pm 9.0 \pm 2.7$	$71.5 \pm 7.8 \pm 3.4$	$82.8 \pm 7.9 \pm 4.0$	$60.8 \pm 10.5 \pm 14.7$
$(1, 2)$	$113.4 \pm 16.2 \pm 6.4$	$127.7 \pm 9.5 \pm 6.0$	$120.8 \pm 7.8 \pm 5.4$	$104.4 \pm 8.3 \pm 4.7$	$91.7 \pm 13.2 \pm 4.6$
$(2, 3)$	$74.3 \pm 7.6 \pm 4.8$	$66.3 \pm 4.2 \pm 3.3$	$62.8 \pm 3.7 \pm 3.1$	$58.2 \pm 3.9 \pm 3.1$	$39.1 \pm 5.7 \pm 2.2$
$(3, 4)$	$32.1 \pm 3.2 \pm 2.2$	$32.8 \pm 2.1 \pm 2.1$	$28.3 \pm 1.8 \pm 1.9$	$22.6 \pm 1.9 \pm 1.7$	$17.5 \pm 3.8 \pm 0.9$
$(4, 5)$	$15.8 \pm 1.8 \pm 1.3$	$14.3 \pm 1.2 \pm 1.2$	$13.2 \pm 1.1 \pm 1.1$	$12.1 \pm 1.2 \pm 1.0$	$15.9 \pm 4.5 \pm 0.9$
$(5, 6)$	$7.24 \pm 1.02 \pm 0.67$	$7.09 \pm 0.75 \pm 0.62$	$4.63 \pm 0.65 \pm 0.51$	$4.33 \pm 0.69 \pm 0.38$	$20.5 \pm 8.2 \pm 17.0$
$(6, 7)$	$4.05 \pm 0.70 \pm 0.41$	$3.92 \pm 0.56 \pm 0.42$	$2.73 \pm 0.46 \pm 0.29$	$2.33 \pm 0.50 \pm 0.24$	—
$(7, 8)$	$1.95 \pm 0.44 \pm 0.20$	$1.92 \pm 0.37 \pm 0.21$	$0.98 \pm 0.27 \pm 0.23$	—-	—

Table 14: D^+ cross-sections in μb in bins of $p_{\rm T}$ and y. The uncertainties given are statistical and uncorrelated systematic uncertainties. Overall correlated relative systematic uncertainties due to tracking (9%), the branching ratio (2.7%), multiple candidates (1%), and luminosity (10%) apply to all bins.

$p_{\rm T}$	y				
(GeV/c)	(2.0, 2.5)	(2.5, 3.0)	(3.0, 3.5)	(3.5, 4.0)	(4.0, 4.5)
(0, 1)	—	$25.1 \pm 4.8 \pm 1.8$	$37.5 \pm 7.6 \pm 2.1$	$57.7 \pm 18.3 \pm 2.9$	$45.5 \pm 15.4 \pm 7.8$
(1, 2)	$54.8 \pm 10.3 \pm 4.1$	$42.2 \pm 3.8 \pm 2.6$	$46.7 \pm 7.2 \pm 2.3$	$61.8 \pm 16.4 \pm 3.8$	$39.1 \pm 12.1 \pm 5.0$
(2, 3)	$31.1 \pm 4.1 \pm 2.0$	$29.6 \pm 2.3 \pm 1.6$	$28.4 \pm 2.6 \pm 1.6$	$23.8 \pm 3.0 \pm 1.7$	$24.4 \pm 5.2 \pm 1.9$
(3, 4)	$13.1 \pm 1.6 \pm 0.8$	$16.0 \pm 1.0 \pm 0.8$	$12.5 \pm 1.0 \pm 0.7$	$9.7 \pm 1.8 \pm 0.6$	$8.7 \pm 1.9 \pm 0.8$
(4, 5)	$7.4 \pm 0.9 \pm 0.9$	$7.9 \pm 0.7 \pm 0.4$	$6.3 \pm 0.6 \pm 0.4$	$5.4 \pm 0.8 \pm 0.4$	$3.2 \pm 0.7 \pm 0.3$
(5, 6)	$5.2 \pm 0.7 \pm 0.3$	$3.1 \pm 0.3 \pm 0.2$	$2.7 \pm 0.3 \pm 0.2$	$1.5 \pm 0.3 \pm 0.1$	$0.3 \pm 0.2 \pm 0.0$
(6, 7)	$2.6 \pm 0.4 \pm 0.2$	$1.5 \pm 0.2 \pm 0.2$	$1.7 \pm 0.2 \pm 0.1$	$0.8 \pm 0.2 \pm 0.1$	—
(7, 8)	$0.8 \pm 0.3 \pm 0.1$	$1.0 \pm 0.2 \pm 0.1$	$0.8 \pm 0.2 \pm 0.1$	$0.5 \pm 0.2 \pm 0.0$	—

Table 15: $D^{*\pm}$ cross-sections in μb in bins of $p_{\rm T}$ and y. The uncertainties given are statistical and uncorrelated systematic uncertainties. Overall correlated relative systematic uncertainties due to tracking (10%), the branching ratio (1.5%), and luminosity (10%) apply to all bins.

$p_{\rm T}$	y				
(GeV/c)	$(2.0, 2.5)$	$(2.5, 3.0)$	$(3.0, 3.5)$	$(3.5, 4.0)$	$(4.0, 4.5)$
$(0, 1)$	—	—	27.1 ± 19.6 $pm2.4$	$43.0 \pm 13.3 \pm 3.9$	$11.2 \pm 14.1 \pm 1.2$
$(1, 2)$	—	$46.1 \pm 18.4 \pm 4.2$	$39.8 \pm 7.3 \pm 3.4$	$45.2 \pm 6.7 \pm 3.9$	$20.6 \pm 8.4 \pm 2.0$
$(2, 3)$	$64.8 \pm 31.5 \pm 8.0$	$34.1 \pm 5.7 \pm 3.1$	$25.6 \pm 3.0 \pm 2.3$	$27.6 \pm 3.3 \pm 2.6$	$11.4 \pm 3.4 \pm 1.2$
$(3, 4)$	$16.4 \pm 7.0 \pm 1.9$	$17.4 \pm 2.4 \pm 1.7$	$14.5 \pm 1.8 \pm 1.5$	$9.89 \pm 1.50 \pm 1.08$	$3.96 \pm 1.26 \pm 0.46$
$(4, 5)$	$9.16 \pm 3.03 \pm 1.12$	$5.83 \pm 1.26 \pm 0.65$	$6.60 \pm 1.02 \pm 0.78$	$5.09 \pm 1.16 \pm 0.65$	$3.05 \pm 1.04 \pm 0.41$
$(5, 6)$	$3.53 \pm 1.28 \pm 0.46$	$4.68 \pm 0.89 \pm 0.56$	$2.05 \pm 0.56 \pm 0.26$	$2.76 \pm 0.68 \pm 0.39$	$0.86 \pm 0.86 \pm 0.13$
$(6, 7)$	$1.37 \pm 0.78 \pm 0.19$	$1.03 \pm 0.39 \pm 0.13$	$1.08 \pm 0.38 \pm 0.15$	$1.61 \pm 0.51 \pm 0.24$	$0.79 \pm 0.99 \pm 0.13$
$(7, 8)$	$1.32 \pm 0.66 \pm 0.19$	$0.71 \pm 0.49 \pm 0.09$	$0.50 \pm 0.31 \pm 0.07$	$0.47 \pm 0.33 \pm 0.07$	—

References

[1] M. Cacciari, S. Frixione, M. Mangano, P. Nason, and G. Ridolfi, private communication.

[2] B.A. Kniehl, G. Kramer, I. Schienbein, and H. Spiesberger, private communication.

[3] **LHCb** Collaboration, "The LHCb Detector at the LHC," *JINST* **3** (2008) S08005.

[4] P. M. Nadolsky *et al.*, "Implications of CTEQ global analysis for collider observables," *Phys. Rev.* **D78** (2008) 013004, arXiv:0802.0007 [hep-ph].

[5] **Particle Data Group** Collaboration, C. Amsler *et al.*, "Fragmentation Functions in e^+e^- Annihilation and Lepton-Nucleon DIS," in "Review of Particle Physics," *Phys. Lett.* **B667** (2008) 1.

[6] J. Pumplin, H. L. Lai, and W. K. Tung, "The Charm Parton Content of the Nucleon," *Phys. Rev.* **D75** (2007) 054029, arXiv:hep-ph/0701220.

[7] T. Kneesch, B. A. Kniehl, G. Kramer, and I. Schienbein, "Charmed-Meson Fragmentation Functions with Finite-Mass Corrections," *Nucl. Phys.* **B799** (2008) 34–59, arXiv:0712.0481 [hep-ph].

[8] B. A. Kniehl and G. Kramer, "Charmed-hadron fragmentation functions from CERN LEP1 revisited," *Phys. Rev.* **D74** (2006) 037502, arXiv:hep-ph/0607306.

[9] T. Sjöstrand, S. Mrenna, and P. Skands, "PYTHIA 6.4 Physics and Manual," *JHEP* **05** (2006) 026, arXiv:hep-ph/0603175.

[10] See footnote 2 of **LHCb** Collaboration, "Prompt K^0_S production in pp collisions at $\sqrt{s} = 0.9$ TeV," *Phys. Lett.* **B693** (2010) 69–80, arXiv:1008.3105 [hep-ex].

[11] I. Belyaev, "Results and prospects for Charm Physics at LHCb," and S. Stone, "First Physics Results from LHCb," presented in *35th International Conference on High Energy Physics (ICHEP2010)*. Paris, France, 2010.

[12] **Particle Data Group** Collaboration, C. Amsler *et al.*, "Review of Particle Physics," *Phys. Lett.* **B667** (2008) 1. and 2009 partial update for the 2010 edition.

[13] **CLEO** Collaboration, J. P. Alexander *et al.*, "Absolute Measurement of Hadronic Branching Fractions of the D_s^+ Meson," *Phys. Rev. Lett.* **100** (2008) 161804, arXiv:0801.0680 [hep-ex].

[14] **LHCb** Collaboration, "Measurement of $\sigma(pp \to b\bar{b}X)$ at $\sqrt{s} = 7$ TeV in the forward region," *Phys. Lett.* **B694** (2010) 209–216, arXiv:1009.2731 [hep-ex].